Transient Aspects of Heat Flux Bifurcation in Porous Media: An Exact Solution

Kun Yang
School of Energy and Power Engineering,
Huazhong University of Science and Technology,
Wuhan 430074, PR China;
Department of Mechanical Engineering,
University of California, Riverside,
Riverside, CA 92521-0425

Kambiz Vafai[1]
Department of Mechanical Engineering,
University of California, Riverside,
Riverside, CA 92521-0425
e-mail: vafai@engr.ucr.edu

The transient thermal response of a packed bed is investigated analytically. A local thermal nonequilibrium model is used to represent the energy transport within the porous medium. The heat flux bifurcation phenomenon in porous media is investigated for temporal conditions and two primary types of heat flux bifurcations in porous media are established. Exact solutions are derived for both the fluid and solid temperature distributions for the constant temperature boundary condition. The fluid, solid, and total Nusselt numbers during transient process are analyzed. A heat exchange ratio is introduced to estimate the influence of interactions between the solid and fluid phases through thermal conduction at the wall within the heat flux bifurcation region. A region where the heat transfer can be described without considering the convection contribution in the fluid phase is found. The two-dimensional thermal behavior for the solid and fluid phases is also analyzed. The temporal temperature differential between the solid and fluid is investigated to determine the domain over which the local thermal equilibrium model is valid. In addition, the characteristic time for reaching steady state conditions is evaluated. [DOI: 10.1115/1.4003047]

Keywords: porous media, heat flux bifurcation, transient heat transfer, local thermal nonequilibrium, analytical solution

1 Introduction

Porous media are used to transport and store energy in many industrial applications such as heat pipe, solid matrix heat exchangers, electronic cooling, and chemical reactors. For a solar collector with air or water as the working fluid, a porous medium can provide an effective means for thermal energy storage. During the period of charging and recovery, transient thermal response aspects of the process for the packed bed are of major concerns.

Local thermal equilibrium (LTE) and local thermal nonequilibrium (LTNE) models are the two primary ways for representing heat transfer in a porous medium. Although LTE model is more convenient to use, more and more studies have suggested that LTE model is not valid for some problems such as storage of thermal energy, or heat transfer in porous media with internal heat generation. In these cases, the LTNE model should be used for solid and fluid phases in porous media [1–3].

Many studies have focused on the transient flow and heat transfer in porous media. Schumann [4] presented an early analytical solution for transient temperature distribution of a semi-infinite porous prism that is initially at a uniform temperature and the sides of the prism were adiabatic. Using a LTNE model, in which the diffusion terms in both the transverse and axial directions were neglected, the fluid and solid temperatures were found as a function of the axial position and time. Riaz [5] investigated the transient response of packed bed thermal storage system, and compared the analytical solutions obtained from simplified LTE and LTNE models, in which Schumann results were used and the transient term in fluid phase was ignored. It is obvious that the transient term in fluid phase should be considered for many types of applications. Spiga and Spiga [6] analytically investigated the dynamic response of porous media and packed beds systems to an arbitrary time varying inlet temperature using a LTNE model, in which the diffusion terms in both the transverse and axial directions were neglected. The temperature responses for step, ramp, and periodic varying inlet temperatures were discussed.

Using a perturbation technique, Kuznetsov [7] presented interesting and important aspects of the temperature difference between solid and fluid phases in a semi-infinite packed bed based on a LTNE model, in which the diffusion terms in transverse directions in both the fluid and solid phases were neglected. Kuznetsov [7] established that the temperature difference between the fluid and solid phases forms a thermal wave localized in space. Using the same technique, Kuznetsov [8] presented an analytical solution for a packed bed subject to a constant temperature condition at the walls, in which the dimensionless solid phase temperature was considered to differ from the fluid phase temperature by a small perturbation. It was shown that the transient component of the temperature difference between the fluid and solid phases describes a wave propagating in the axial direction from the fluid inlet boundary.

Hendal et al. [9] presented an analytical solution for the transient thermal behavior of a two dimensional circulating porous bed based on a LTE model. Their findings showed that the temperature propagates throughout the bed in a wavelike form and approach steady state results for large values of time. Beasley and Clark [10] developed a numerical model to predict the transient response of a packed bed based on the LTNE model, in which the diffusion terms in both the transverse and axial directions in the solid phase were neglected. Their numerical results compared favorably with the experimental measurement of temperature distribution in a packed bed of uniform spheres with air as working fluid. Amiri and Vafai [3] presented a comprehensive investigation of the transient response within a packed bed. The temporal impact of the non-Darcian terms and the thermal dispersion effects on energy transport were investigated, and the range of the validity for LTE condition was established in detail.

In the present work, the LTNE model is employed to represent the energy transport within a porous medium. Two primary types of heat flux bifurcations in porous media are investigated for tem-

[1]Corresponding author.

Contributed by the Heat Transfer Division of ASME for publication in the JOURNAL OF HEAT TRANSFER. Manuscript received September 7, 2010; final manuscript received October 31, 2010; published online February 4, 2011. Assoc. Editor: Oronzio Manca.

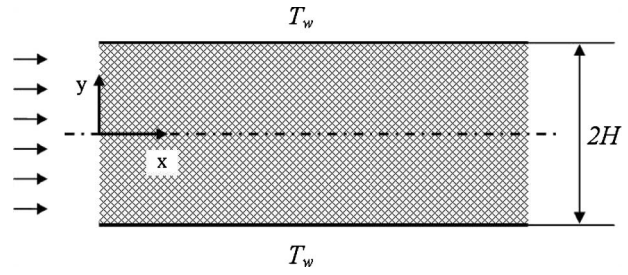

Fig. 1 Schematic diagram for transport through a channel filled with a porous medium and the corresponding coordinate system

poral conditions. Heat transfer performances in terms of the fluid, solid, and total Nusselt number are presented. Qualitative analyses of the effects of thermal conduction at the wall on the total heat exchange between the solid and fluid phases within the heat flux bifurcation region are also performed. Both the transient and diffusion aspects are considered in the solid and fluid phases along with the convection and the fluid-solid interaction. The analytical solution for transient response of a packed bed subject to a constant temperature boundary condition is derived. The heat flux bifurcation phenomenon in porous media is investigated for temporal conditions, and the analytical two-dimensional thermal behavior and the LTE model is examined under transient conditions. Furthermore, the response time toward steady state conditions is investigated.

2 Modeling and Formulation

The schematic diagram of the problem is shown in Fig. 1. Fluid flows through a rectangular channel filled with a porous medium subject to a constant temperature boundary condition. The height of the channel is $2H$ and the temperature at the wall is T_w. The following assumptions are invoked in the analyzing this problem.

(1) The flow is incompressible and represented by the Darcian flow model.
(2) Natural convection and radiative heat transfer are negligible.
(3) Axial heat conduction in both the solid and fluid phases are negligible.
(4) Properties such as specific heat, density, and thermal conductivity, as well as porosity are assumed to be constant.

2.1 Governing Equation and Boundary and Initial Conditions. Based on these assumptions, the following governing equations are obtained from the work of Amiri and Vafai [3] employing the local thermal nonequilibrium model.

Fluid phase

$$\beta\frac{\partial\theta_f}{\partial\tau}+\frac{\partial\theta_f}{\partial\xi}=k\frac{\partial^2\theta_f}{\partial\eta^2}+(\theta_s-\theta_f) \tag{1}$$

Solid phase

$$\frac{\partial\theta_s}{\partial\tau}=\frac{\partial^2\theta_s}{\partial\eta^2}-(\theta_s-\theta_f) \tag{2}$$

Boundary conditions

$$\theta_f|_{\eta=\eta_1}=\theta_s|_{\eta=\eta_1}=0 \tag{3a}$$

$$\left.\frac{\partial\theta_f}{\partial\eta}\right|_{\eta=0}=\left.\frac{\partial\theta_s}{\partial\eta}\right|_{\eta=0}=0 \tag{3b}$$

$$\theta_f|_{\xi=0}=\theta_{in} \tag{3c}$$

Initial conditions

$$\theta_f|_{\tau=0}=\theta_s|_{\tau=0}=1 \tag{4}$$

where

$$\xi=\frac{xh_i\alpha}{\rho_f c_f u}\qquad \tau=\frac{t}{(1-\varepsilon)\rho_s c_s/(h_i\alpha)}$$

$$\eta=\frac{y}{\sqrt{k_{s,eff}/(h_i\alpha)}},\quad \eta_1=\frac{H}{\sqrt{k_{s,eff}/(h_i\alpha)}}=\sqrt{Bi}\quad where\quad Bi=\frac{h_i\alpha H^2}{k_{s,eff}}$$

$$\beta=\frac{\varepsilon\rho_f c_f}{(1-\varepsilon)\rho_s c_s},\quad k=\frac{k_{f,eff}}{k_{s,eff}},\quad \theta=\frac{T-T_w}{T_0-T_w} \tag{5}$$

2.2 Solution Methodology. The nondimensional fluid and solid temperature distributions, $\theta_f(\xi,\eta,\tau)$ and $\theta_s(\xi,\eta,\tau)$ are represented as

$$\theta_f(\xi,\eta,\tau)=U_f(\xi,\tau)V(\eta) \tag{6}$$

$$\theta_s(\xi,\eta,\tau)=U_s(\xi,\tau)V(\eta) \tag{7}$$

Substituting Eqs. (6) and (7) into Eqs. (1) and (2) along with the boundary conditions and applying the separation of variables and Laplace transformation yield

$$\theta_f(\xi,\eta,\tau)=\sum_{n=0}^{\infty}U_{fn}(\xi,\tau)\cos(s_n\eta) \tag{8}$$

$$\theta_s(\xi,\eta,\tau)=\sum_{n=0}^{\infty}U_{sn}(\xi,\tau)\cos(s_n\eta) \tag{9}$$

where

$$s_n=\frac{(n+0.5)\pi}{\eta_1},\quad n=0,1,2,\ldots \tag{10}$$

$$\beta mW_{fn}-\beta\frac{2\sin(s_n\eta_1)}{s_n\eta_1}+\frac{\partial W_{fn}}{\partial\xi}-(W_{sn}-W_{fn})=-s_n^2kW_{fn} \tag{11}$$

$$mW_{sn}-\frac{2\sin(s_n\eta_1)}{s_n\eta_1}+(W_{sn}-W_{fn})=-s_n^2W_{sn} \tag{12}$$

where W_{sn} and W_{fn} are the Laplace transformations of U_{sn} and U_{fn}, respectively, given by

$$W_{sn}=\int_0^{\infty}U_{sn}e^{-m\tau}d\tau \tag{13}$$

$$W_{fn}=\int_0^{\infty}U_{fn}e^{-m\tau}d\tau \tag{14}$$

Solving Eqs. (11) and (12) yields

$$W_{fn}=\left[\frac{\theta_{in}}{m}-\frac{\beta(1+m+s_n^2)+1}{(\beta m+s_n^2k+1)(1+m+s_n^2)-1}\right]\frac{2\sin(s_n\eta_1)}{s_n\eta_1}\times\exp\left[-\left(\beta m+s_n^2k+1-\frac{1}{1+m+s_n^2}\right)\xi\right]+\frac{\beta(1+m+s_n^2)+1}{(\beta m+s_n^2k+1)(1+m+s_n^2)-1}\frac{2\sin(s_n\eta_1)}{s_n\eta_1} \tag{15}$$

By utilizing inverse Laplace transform, U_{sn} and U_{fn} are obtained as

$$U_{sn}=(\theta_{s1}+\theta_{s2}+\theta_{s3}+\theta_{s4}+\theta_{s5}+\theta_{s6})\frac{2\sin(s_n\eta_1)}{s_n\eta_1} \tag{16}$$

$$U_{fn} = (\theta_{f1} + \theta_{f2} + \theta_{f3} + \theta_{f4} + \theta_{f5})\frac{2\sin(s_n\eta_1)}{s_n\eta_1} \tag{17}$$

where

$$\theta_{s1} = \theta_{in} f(p_0)$$

$$\theta_{s2} = -\left(\frac{p_1}{p_1 - p_2} + \frac{\beta s_n^2 + \beta + 1}{\beta(p_1 - p_2)}\right) f(p_1)$$

$$\theta_{s3} = -\left(\frac{p_2}{p_2 - p_1} + \frac{\beta s_n^2 + \beta + 1}{\beta(p_2 - p_1)}\right) f(p_2)$$

$$\theta_{s4} = \left[\frac{1}{p_1 - p_2} + \frac{1}{\beta(p_1 - p_2)(p_1 + s_n^2 + 1)}\right]\exp(p_1\tau)$$

$$\theta_{s5} = \left[\frac{1}{p_2 - p_1} + \frac{1}{\beta(p_2 - p_1)(p_2 + s_n^2 + 1)}\right]\exp(p_2\tau)$$

$$\theta_{s6} = \left[1 + \frac{1}{\beta(p_1 + s_n^2 + 1)(p_2 + s_n^2 + 1)}\right]\exp[-(s_n^2 + 1)\tau]$$

$$\theta_{f1} = \theta_{in} g(p_0)$$

$$\theta_{f2} = -\left(\frac{p_1}{p_1 - p_2} + \frac{\beta s_n^2 + \beta + 1}{\beta(p_1 - p_2)}\right) g(p_1)$$

$$\theta_{f3} = -\left(\frac{p_2}{p_2 - p_1} + \frac{\beta s_n^2 + \beta + 1}{\beta(p_2 - p_1)}\right) g(p_2)$$

$$\theta_{f4} = \left[\frac{p_1}{p_1 - p_2} + \frac{\beta s_n^2 + \beta + 1}{\beta(p_1 - p_2)}\right]\exp(p_1\tau)$$

$$\theta_{f5} = \left[\frac{p_2}{p_2 - p_1} + \frac{\beta s_n^2 + \beta + 1}{\beta(p_2 - p_1)}\right]\exp(p_2\tau)$$

$$f(p) = \exp[-(ks_n^2 + 1)\xi + p(\tau - \beta\xi)]\int_0^\tau I_0(2\sqrt{\xi t_1})\exp[-(s_n^2 + 1 + p)t_1]Q(\tau - t_1 - \beta\xi)dt_1$$

$$g(p) = \exp[-(ks_n^2 + 1)\xi + p(\tau - \beta\xi)]\int_0^\tau \sqrt{\frac{\xi}{\tau}} I_1(2\sqrt{\xi t_1})\exp[-(s_n^2 + 1 + p)t_1]Q(\tau - t_1 - \beta\xi)dt_1 + \exp[-(ks_n^2 + 1)\xi + p(\tau - \beta\xi)]Q(\tau - \beta\xi)$$

where $Q(\tau)$ is the unit step function,

$$Q(\tau) = \begin{cases} 1, & \tau > 0 \\ 0, & \tau < 0 \end{cases}$$

and

$$p_0 = 0$$

$$p_1 = \frac{-(\beta s_n^2 + \beta + ks_n^2 + 1) + \sqrt{(\beta s_n^2 + \beta - ks_n^2 - 1)^2 + 4\beta}}{2\beta}$$

$$p_2 = \frac{-(\beta s_n^2 + \beta + ks_n^2 + 1) - \sqrt{(\beta s_n^2 + \beta - ks_n^2 - 1)^2 + 4\beta}}{2\beta} \tag{18}$$

By substituting Eqs. (16) and (17) in Eqs. (8) and (9), the final resulting solutions for Eqs. (1), (2), (3*a*)–(3*c*), and (4) are obtained as

$$\theta_s = \frac{2}{\eta_1}\sum_{n=0}^{\infty}(\theta_{s1} + \theta_{s2} + \theta_{s3} + \theta_{s4} + \theta_{s5} + \theta_{s6})\frac{\sin(s_n\eta_1)}{s_n}\cos(s_n\eta) \tag{19}$$

$$\theta_f = \frac{2}{\eta_1}\sum_{n=0}^{\infty}(\theta_{f1} + \theta_{f2} + \theta_{f3} + \theta_{f4} + \theta_{f5})\frac{\sin(s_n\eta_1)}{s_n}\cos(s_n\eta) \tag{20}$$

The average temperature can be calculated from

$$\theta_s^a = \frac{1}{\eta_1}\int_0^{\eta_1}\theta_s d\eta \tag{21}$$

$$\theta_f^a = \frac{1}{\eta_1}\int_0^{\eta_1}\theta_f d\eta \tag{22}$$

Substituting Eqs. (19) and (20) into Eqs. (21) and (22) yields

$$\theta_s^a = \frac{2}{\eta_1^2}\sum_{n=0}^{\infty}(\theta_{s1} + \theta_{s2} + \theta_{s3} + \theta_{s4} + \theta_{s5} + \theta_{s6})\frac{1}{s_n^2} \tag{23}$$

$$\theta_f^a = \frac{2}{\eta_1^2}\sum_{n=0}^{\infty}(\theta_{f1} + \theta_{f2} + \theta_{f3} + \theta_{f4} + \theta_{f5})\frac{1}{s_n^2} \tag{24}$$

2.3 Steady State Solution. The governing equations for steady state conditions can be obtained from Eqs. (1) and (2) by deleting the transient term. This results in

$$\theta_{ss} = \frac{2\theta_{in}}{\eta_1}\sum_{n=0}^{\infty}\exp\left[-\left(ks_n^2 + 1 - \frac{1}{s_n^2 + 1}\right)\xi\right]\frac{\sin(s_n\eta_1)}{s_n(s_n^2 + 1)}\cos(s_n\eta) \tag{25}$$

$$\theta_{fs} = \frac{2\theta_{in}}{\eta_1}\sum_{n=0}^{\infty}\exp\left[-\left(ks_n^2 + 1 - \frac{1}{s_n^2 + 1}\right)\xi\right]\frac{\sin(s_n\eta_1)}{s_n}\cos(s_n\eta) \tag{26}$$

and the average temperature under steady state conditions are obtained as

$$\theta_{ss}^a = \frac{2\theta_{in}}{\eta_1^2}\sum_{n=0}^{\infty}\exp\left[-\left(ks_n^2 + 1 - \frac{1}{s_n^2 + 1}\right)\xi\right]\frac{1}{s_n^2(s_n^2 + 1)} \tag{27}$$

$$\theta_{fs}^a = \frac{2\theta_{in}}{\eta_1^2}\sum_{n=0}^{\infty}\exp\left[-\left(ks_n^2 + 1 - \frac{1}{s_n^2 + 1}\right)\xi\right]\frac{1}{s_n^2} \tag{28}$$

2.4 Solution for the Case Without the Convective Term in the Fluid Phase. The governing equations for the case without the convective contribution in the fluid phase can be obtained from Eqs. (1) and (2). This results in

$$\theta_{sNC} = \frac{2}{\eta_1}\sum_{n=0}^{\infty}(\theta_{s4} + \theta_{s5} + \theta_{s6})\frac{\sin(s_n\eta_1)}{s_n}\cos(s_n\eta) \tag{29}$$

$$\theta_{fNC} = \frac{2}{\eta_1}\sum_{n=0}^{\infty}(\theta_{f4} + \theta_{f5})\frac{\sin(s_n\eta_1)}{s_n}\cos(s_n\eta) \tag{30}$$

The average temperatures for the case without the convective contribution in the fluid phase are obtained as

$$\theta_{sNC}^a = \frac{2}{\eta_1^2}\sum_{n=0}^{\infty}(\theta_{s4} + \theta_{s5} + \theta_{s6})\frac{1}{s_n^2} \tag{31}$$

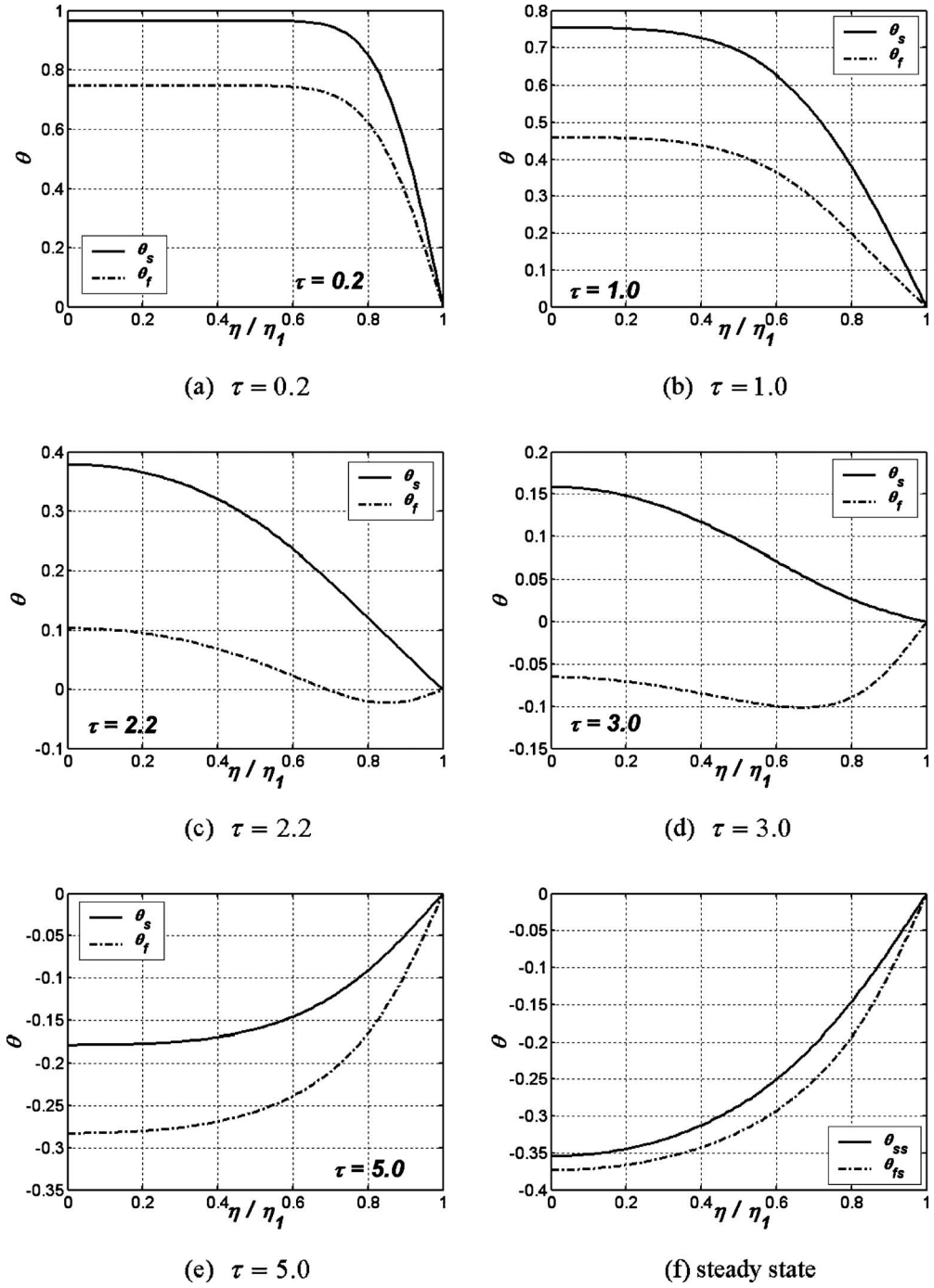

Fig. 2 Dimensionless temperature distributions for fluid and solid phases for k=0.1, β=0.02, η_1 =5, ξ=2, and θ_{in}=−0.4: (*a*) τ=0.2, (*b*) τ=1.0, (*c*) τ=2.2, (*d*) τ=3.0, (*e*) τ=5.0, and (*f*) steady state

$$\theta_{fNC}^{a} = \frac{2}{\eta_1^2}\sum_{n=0}^{\infty}(\theta_{f4} + \theta_{f5})\frac{1}{s_n^2} \tag{32}$$

3 Results and Discussion

The dimensionless temperature distributions for the fluid and solid phases are shown in the Fig. 2. When τ is small, the temperature distribution is mainly dependent on the initial condition. However, when τ is large enough, the temperature distribution is primarily dependent on the inlet condition. Although the temperature difference between the fluid and solid phases is relatively small when steady state conditions are reached, it is relatively large compared with the fluid and solid temperatures during the transient process. These results show that the LTE model might be unsuitable to describe the transient heat transfer process in porous media. This figure also discloses that the thermal boundary layer grows as τ increases, which indicates a substantial two-dimensional thermal characteristic.

It is important to note that the direction of the temperature gradient for the fluid and solid phases are different at the wall (η= η_1) in Figs. 2(*c*) and 2(*d*). This leads to a heat flux bifurcation around these times. The concept of temperature gradient bifurcation in the presence of internal heat generation in both the fluid and solid phases has been established in detail for the first time by

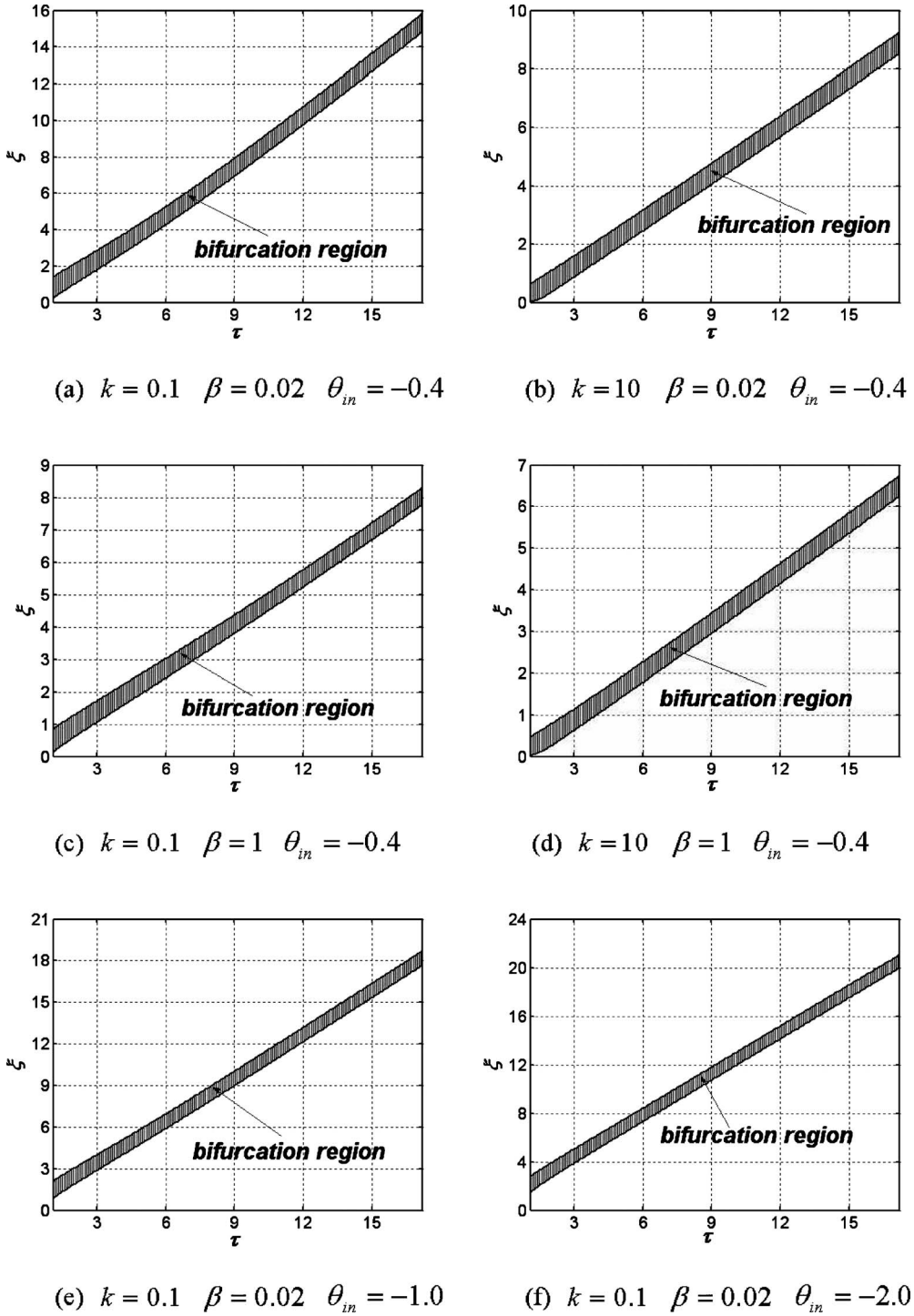

Fig. 3 Bifurcation region variations as a function of pertinent parameters β, k, and θ_{in}

Yang and Vafai [11]. Utilizing the analytical solutions given in Eqs. (19) and (20), the region over which heat flux bifurcation phenomenon occurs is established and illustrated in Fig. 3. It is found that this phenomenon occurs only over a given axial region at a given time frame. The bifurcation region moves downstream as τ increases, and is dependent on the pertinent parameters k, β, and θ_{in}. When k, β, and θ_{in} decrease, the bifurcation region moves forward at a faster rate. It should be noted that bifurcation phenomenon only occurs during the transient period. Bifurcation phenomenon disappears when steady state conditions are reached. It should be noted that the bifurcation aspects related to phase change as analyzed in Ref. [12] have not been investigated in this work.

The dimensionless transverse average temperature distributions for fluid and solid phases for k=0.1, β=0.02, η_1=5, and θ_{in}= −0.4 are shown in Fig. 4. It is found that the transverse average temperatures approach the case with no convection in the fluid phase when the axial length is large enough. Based on Eqs. (19), (20), (29), and (30), if ξ satisfies the condition

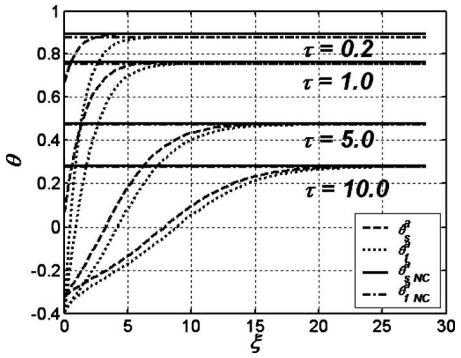

Fig. 4 Dimensionless transverse average temperature distributions for fluid and solid phases for k=0.1, β=0.02, η_1=5, and θ_{in}=−0.4

$$\xi > \frac{\tau}{\beta} \tag{33}$$

convection will have an insignificant impact on the temperature distributions for fluid and solid phases. This is because that the inlet condition effects do not propagate far enough to influence that time level.

The difference between θ_s^a and θ_{ss}^a presents the transient component of the average solid temperature θ_s^a, and the difference between θ_f^a and θ_{fs}^a presents the transient component of the average fluid temperature θ_f^a. These differences are shown in Fig. 5 for k=0.1, β=0.02, η_1=5, and θ_{in}=−0.4. It is found that the peak positions for the transient components of the solid and fluid phases moves downstream with time, while the magnitude of the peak decreases with time.

The transverse average temperature difference distributions between the solid and fluid phases for k=0.1, β=0.02, η_1=10, and θ_{in}=−0.4 is shown in Fig. 6. It is found that there is a peak for the temperature difference at a given τ, and that the peak moves downstream as time progresses. For unsteady flow of a gas through a porous medium, Vafai and Sozen [13] utilized the maximum difference between the solid and fluid phase temperatures to establish the validity of local thermal equilibrium assumption. It was found that the local thermal equilibrium assumption becomes more viable as both the Darcy and particle Reynolds numbers decrease. They had shown that a decrease in the Darcy number translates into a decrease in the particle diameter, which results in an increase in the specific surface area (α), thus increasing the fluid-to-solid heat transfer interaction by offering a larger surface area. Furthermore, as the fluid velocity increases the time for the

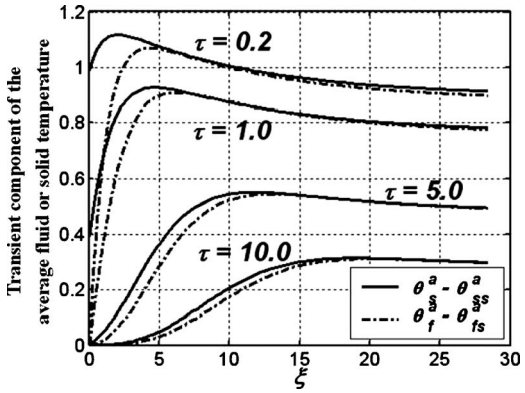

Fig. 5 Variations of the transient component of the average temperature for fluid and solid phases for k=0.1, β=0.02, η_1=5, and θ_{in}=−0.4

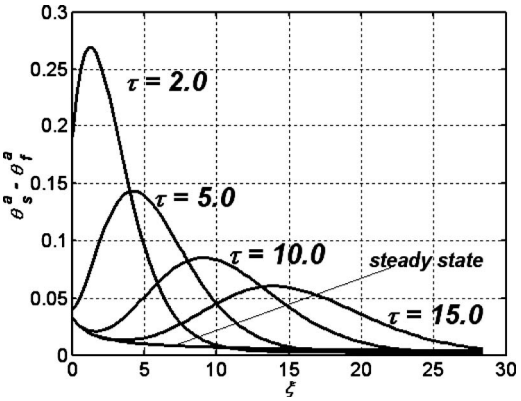

Fig. 6 Spatial and temporal variations of the average temperature difference between the solid and fluid phases for k=0.1, β=0.02, η_1=10, and θ_{in}=−0.4

solid-to-fluid heat exchange interaction decreases, resulting in a decrease in the efficiency of heat exchange between the solid and fluid phases, thus increasing the deviation from the local thermal equilibrium. Similarly here based on the definition of ξ given in Eq. (5), an increase in the specific surface area (α) and a decrease in the fluid velocity can be translated into an increase in ξ. As such the temperature difference between the solid and fluid phases becomes smaller at larger value of ξ, as can be seen in Fig. 6.

The time τ_s or τ_f that it takes for either the solid or fluid phase to reach steady state condition is based on when the quantities defined by

$$\left| \frac{\theta_s^a(\xi,\tau_s) - \theta_{ss}^a(\xi)}{\theta_{ss}^a(\xi)} \right| = 0.01 \tag{34a}$$

$$\left| \frac{\theta_f^a(\xi,\tau_f) - \theta_{fs}^a(\xi)}{\theta_{fs}^a(\xi)} \right| = 0.01 \tag{34b}$$

are achieved, respectively.

The characteristic times for solid and fluid phases to reach steady state are shown in Fig. 7. As can be seen, the characteristic time for the solid is always larger than that for the fluid phase. It can also be seen that the characteristic times increase as k, β, η_1, or θ_{in} increase. It is found that the characteristic times remain almost unchanged with k at any given ξ when $k<1$. This is due to the negligible influence of the fluid thermal conduction.

4 Nusselt Number Results

The Nusselt numbers for fluid and solid phases can be presented as

$$\mathrm{Nu}_f = -\frac{4\eta_1}{\theta_f^a}\left(\frac{\partial\theta_f}{\partial\eta}\right)_{\eta=\eta_1} \tag{35}$$

$$\mathrm{Nu}_s = -\frac{4\eta_1}{\theta_f^a k}\left(\frac{\partial\theta_s}{\partial\eta}\right)_{\eta=\eta_1} \tag{36}$$

The Nusselt numbers for fluid and solid phases are presented along the axial coordinate in Fig. 8. It can be seen that the Nusselt numbers approach infinity at a specific axial location at any given time up to approximately when the steady state conditions are reached. It is also found that, far enough downstream of the entrance, the Nusselt number becomes invariant with position. This phenomenon occurs when the dimensional wall temperature value is within the range specified by the initial and inlet temperature values. This is the reason why this phenomenon did not occur in the work of Amiri and Vafai [3]. In their work, the wall temperature was larger than the entrance and the initial temperature. As

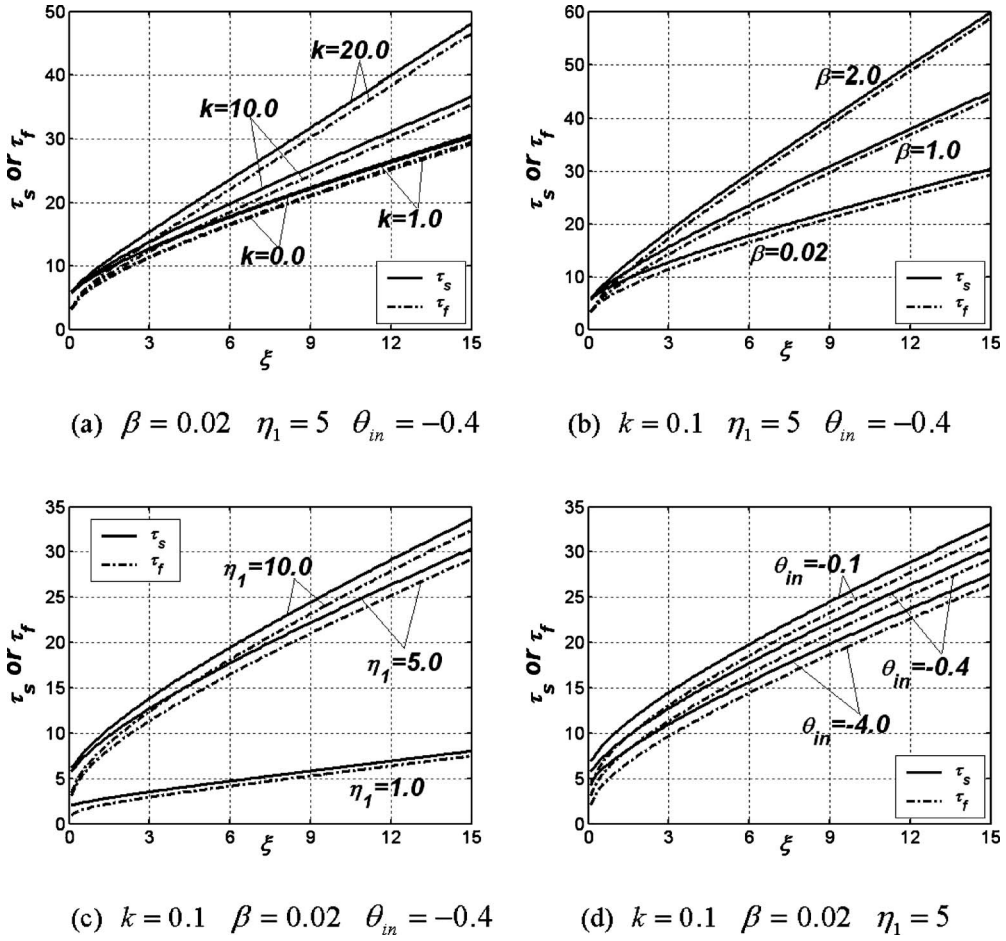

Fig. 7 Characteristic time variations of the solid and fluid phases as a function of pertinent parameters k, β, η_1, and θ_{in}

such in their work the dimensionless average temperature did not approach a zero value. Furthermore, it should be noted this phenomenon is a manifestation of nondimensional temperature quantities.

The fully developed temperature distributions for fluid and solid phases under steady state conditions can be derived from Eqs. (25) and (26),

$$\theta_{fs\_d} = \frac{2\theta_{in}}{\eta_1}\exp\left[-\left(ks_0^2+1-\frac{1}{s_0^2+1}\right)\xi\right]\frac{\sin(s_0\eta_1)}{s_0}\cos(s_0\eta) \tag{37}$$

$$\theta_{ss\_d} = \frac{2\theta_{in}}{\eta_1}\exp\left[-\left(ks_0^2+1-\frac{1}{s_0^2+1}\right)\xi\right]\frac{\sin(s_0\eta_1)}{s_0(s_0^2+1)}\cos(s_0\eta) \tag{38}$$

Furthermore, the average fully developed temperature distributions for fluid and solid under steady state conditions can be obtained as

$$\theta^a_{fs\_d} = \frac{2\theta_{in}}{\eta_1^2}\exp\left[-\left(ks_0^2+1-\frac{1}{s_0^2+1}\right)\xi\right]\frac{1}{s_0^2} \tag{39}$$

$$\theta^a_{ss\_d} = \frac{2\theta_{in}}{\eta_1^2}\exp\left[-\left(ks_0^2+1-\frac{1}{s_0^2+1}\right)\xi\right]\frac{1}{s_0^2(s_0^2+1)} \tag{40}$$

By utilizing Eqs. (37)–(40), the following equations is obtained:

$$\frac{\theta_{ss\_d}}{\theta^a_{ss\_d}} = \frac{\theta_{fs\_d}}{\theta^a_{fs\_d}} = \frac{\pi}{2}\cos(s_0\eta) = \frac{T_{fs\_d}-T_w}{T^a_{fs\_d}-T_w} = \frac{T_{ss\_d}-T_w}{T^a_{ss\_d}-T_w} \tag{41}$$

As such the dimensionless fully developed temperature distributions, $(T_{fs\_d}-T_w)/(T^a_{fs\_d}-T_w)$ and $(T_{ss\_d}-T_w)/(T^a_{ss\_d}-T_w)$, become independent of the axial length when condition given by Eq. (39) is achieved. By utilizing Eqs. (37)–(39), the fully developed Nusselt numbers for fluid and solid phases under steady state condition are obtained as

$$\mathrm{Nu}_{fs\_d} = \pi^2 \tag{42}$$

$$\mathrm{Nu}_{ss\_d} = \frac{4\eta_1^2\pi^2}{k(\pi^2+4\eta_1^2)} \tag{43}$$

Defining a total Nusselt number, which is the sum of Nu_f and Nu_s, we obtain

$$\mathrm{Nu}_{ts\_d} = \mathrm{Nu}_{fs\_d} + \mathrm{Nu}_{ss\_d} = \frac{4\eta_1^2\pi^2}{k(\pi^2+4\eta_1^2)} + \pi^2 \tag{44}$$

As can be seen, the total fully developed Nusselt number under steady state condition increases with η_1, which is directly related to the Biot number, and decreases with the thermal conductivity ratio, k.

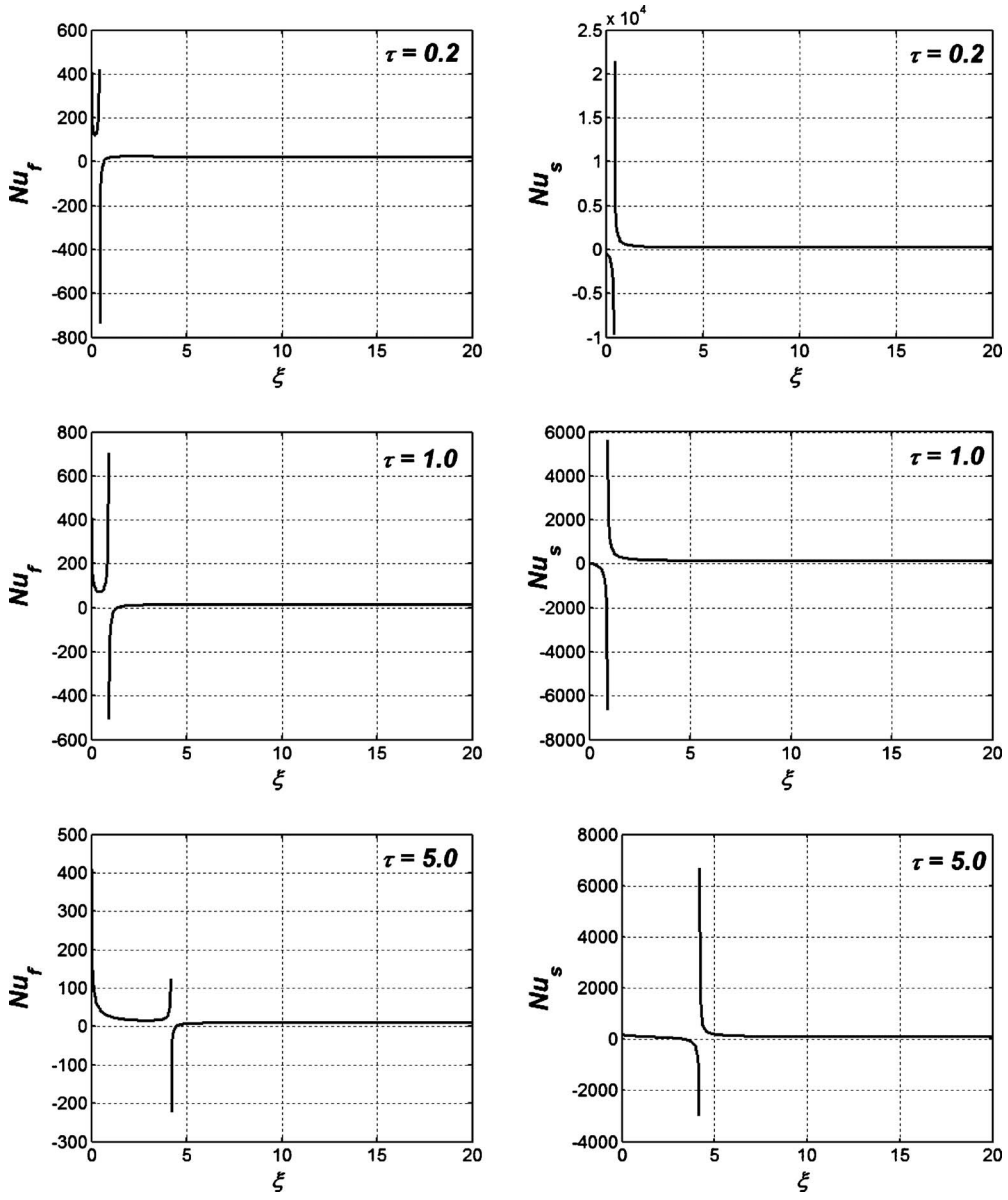

Fig. 8 Nusselt number distributions for fluid and solid phases for k=0.1, β=0.02, η_1=5, and θ_{in} =−0.4

5 Two Primary Types of Heat Flux Bifurcations in Porous Media

In what follows, we demonstrate the existence of two types of heat flux bifurcations in porous media. The first type is the same as the one discussed by Yang and Vafai [11]. For the second type of heat flux bifurcation, we start with representation of the total heat flux at the wall as

$$q_w = -k_{f,\text{eff}}\left(\frac{\partial T_f}{\partial y}\right)_{y=H} - k_{s,\text{eff}}\left(\frac{\partial T_s}{\partial y}\right)_{y=H} \tag{45}$$

The dimensionless total heat flux at the wall is obtained from

$$\Omega_w = \frac{q_w}{(T_0 - T_w)\sqrt{k_{s,\text{eff}} h_i \alpha}} = -k\left(\frac{\partial \theta_f}{\partial \eta}\right)_{\eta=\eta_1} - \left(\frac{\partial \theta_s}{\partial \eta}\right)_{\eta=\eta_1} \tag{46}$$

The dimensionless total heat flux at the wall for k=0.1, β =0.02, η_1=5, and θ_{in}=−0.4 is shown in Fig. 9. It is found that the direction of total heat flux changes along the channel. This leads to a different type of heat flux bifurcation. This bifurcation must

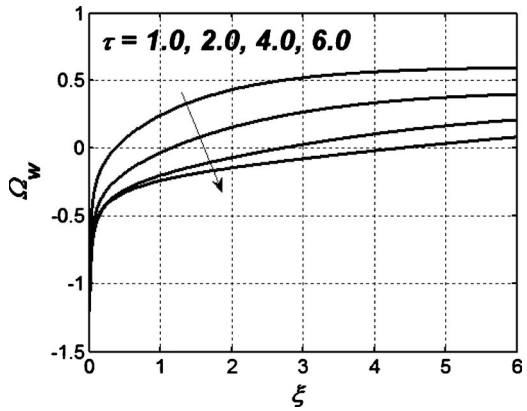

Fig. 9 Dimensionless total heat flux at the wall for k=0.1, β =0.02, η_1=5, and θ_{in}=−0.4

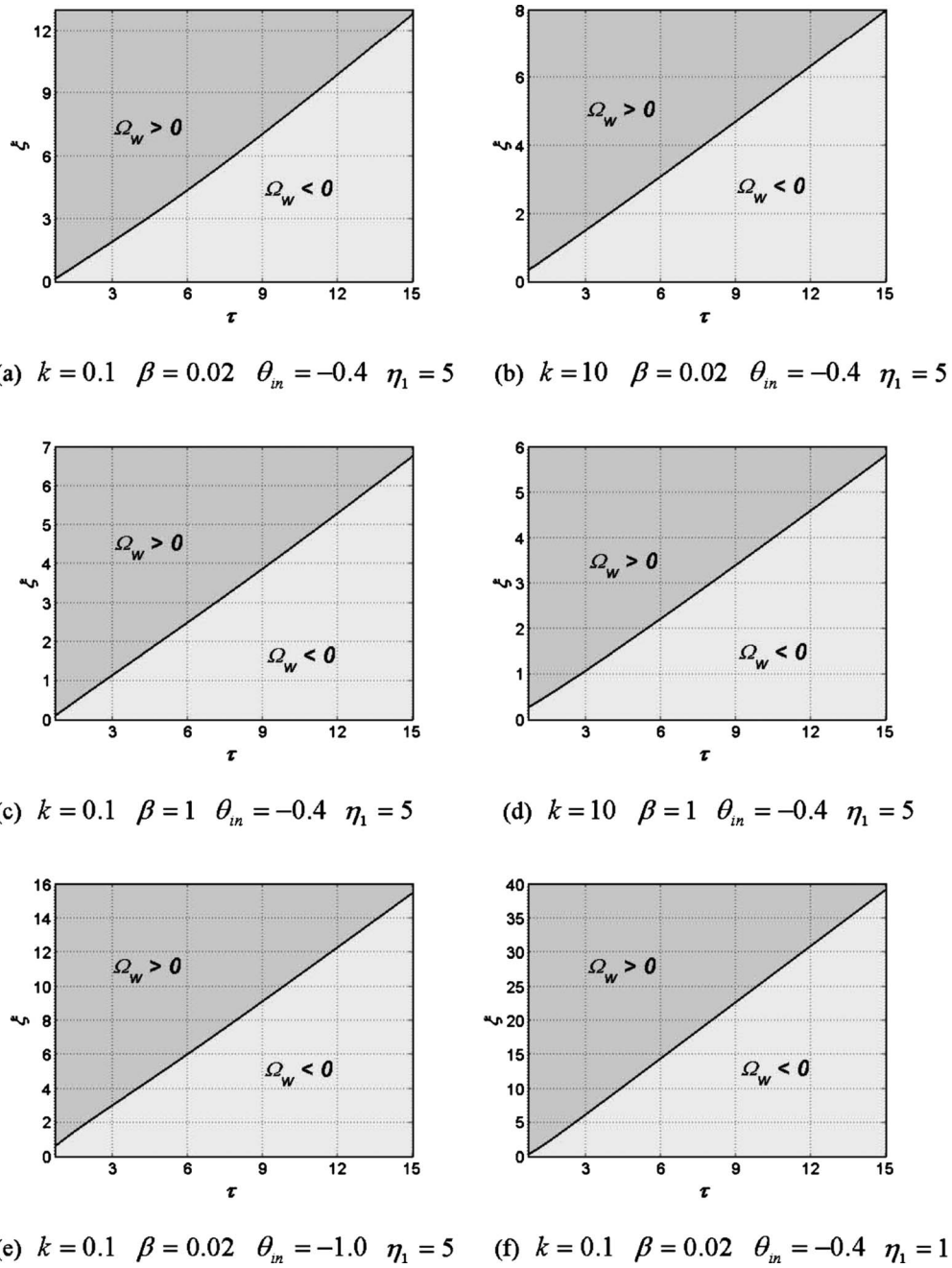

Fig. 10 An example of the requirement to change the imposed heat flux direction at the wall, due to the bifurcation effect, to obtain a constant temperature condition

be taken into account for various applications, where there is a need to maintain a constant temperature boundary condition. As shown in Fig. 10, the total heat flux bifurcation region changes with time, and is dependent on the pertinent parameters k, β, η_1, and θ_{in}. It should be noted that this type of bifurcation phenomenon only occurs during the transient process. The interface line between the regions $\Omega_w > 0$ and $\Omega_w < 0$ represents the location for $\Omega_w = 0$, which moves downstream with time. The speed, which the bifurcation region moves downstream, increases as either k, β, η_1, or θ_{in} decreases. When $q_w = 0$, the heat exchange between the solid and fluid phases through thermal conduction at the wall is obtained from

$$Q_o = \left| -k_{f,\text{eff}} \left(\frac{\partial T_f}{\partial y} \right)_{y=H} \right| = \left| k_{s,\text{eff}} \left(\frac{\partial T_s}{\partial y} \right)_{y=H} \right| \tag{47}$$

The integrated internal heat exchange between the solid and fluid phases can be calculated from

$$Q_i = \left| \int_0^H h_i \alpha (T_s - T_f) dy \right| = \left| h_i \alpha H (T_0 - T_w)(\theta_s^a - \theta_f^a) \right| \tag{48}$$

The corresponding heat exchange ratio is defined as

$$\gamma = \frac{Q_o}{Q_i + Q_o} \tag{49}$$

The heat exchange ratio variations as a function of parameters η_1, k, θ_{in}, and β for $q_w = 0$ are shown in Fig. 11. It is found that the heat exchange ratio is mostly dependent on η_1 and k, whereas θ_{in} and β have little influence on the heat exchange ratio. The heat

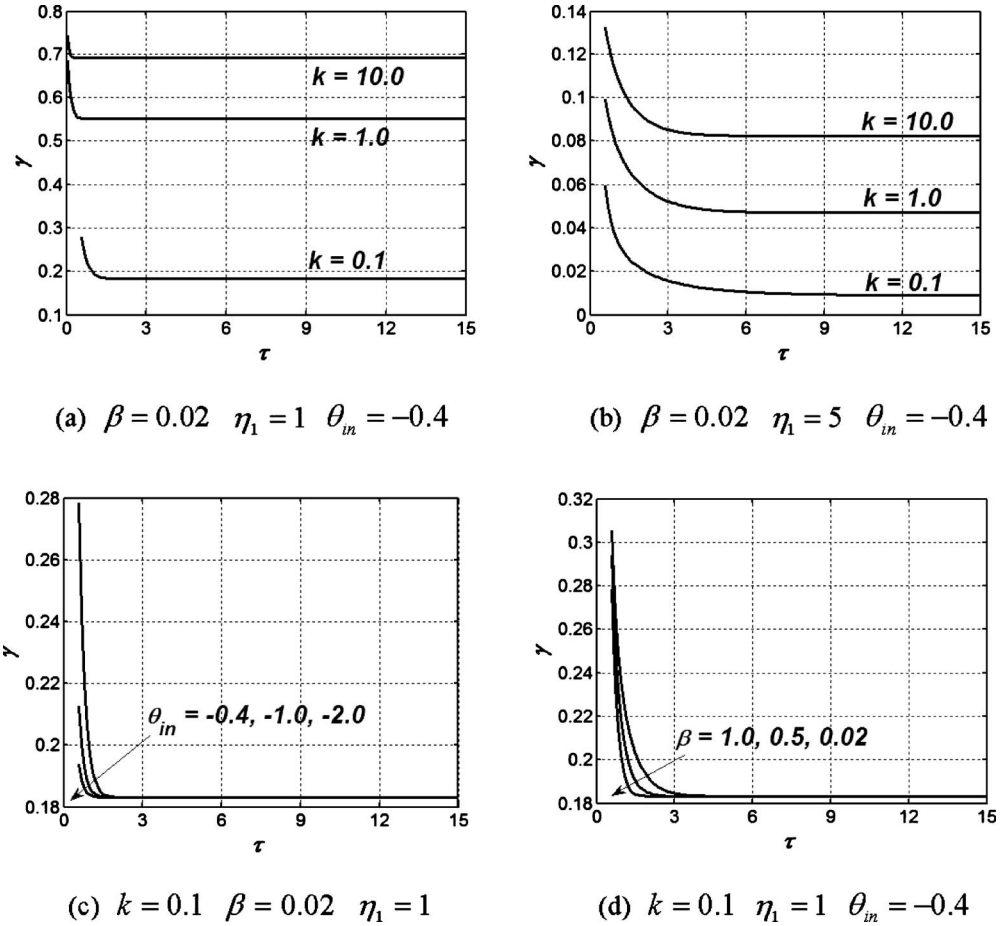

Fig. 11 Heat exchange ratio variations as a function of pertinent parameters η_1, k, θ_{in}, and β for $q_w=0$

exchange between solid and fluid phases through the thermal conduction at the wall is more prominent for small η_1 and large k. When $\eta_1=1$ and $k=10$, up to 68% of total heat exchange between solid and fluid phases within the bifurcation region is through thermal conduction at the wall. It should be noted that the temporal variations of the heat exchange ratio displays two distinct regimes. During the initial stage, the heat exchange ratio decreases sharply with time, while for the later stage, the heat exchange ratio remains almost unchanged.

When $q_w \neq 0$, for the region where the first type of heat flux bifurcation occurs, the heat exchange between the solid and fluid phases through the thermal conduction at the wall can be represented as

$$Q_o = \min\left\{\left|-k_{f,\text{eff}}\left(\frac{\partial T_f}{\partial y}\right)_{y=H}\right|, \left|-k_{s,\text{eff}}\left(\frac{\partial T_s}{\partial y}\right)_{y=H}\right|\right\} \quad \text{for} \quad \left(\frac{\partial T_f}{\partial y}\right)_{y=H}\left(\frac{\partial T_s}{\partial y}\right)_{y=H} < 0 \tag{50}$$

The corresponding heat exchange ratio for $q_w \neq 0$ is also calculated using Eq. (49), and shown in Fig. 12. The dashed line in Fig. 12 represents the maxima loci of the heat exchange ratio. Comparing Figs. 10(*a*), 11(*b*), and 12, it is found that this dashed line is identical to the corresponding curve for $k=0.1$ shown in Fig. 11(*b*), which implies that the heat exchange ratio for $q_w \neq 0$ is always smaller than the corresponding one for $q_w=0$.

As an example, the dimensional characteristic time was calculated for sandstone while the working fluid is air. The following physical data were used: $T_{in}=300$ K, $T_w=310$ K, $T_o=335$ K, $H=0.05$ m, $d_p=5$ mm, and $\varepsilon=0.391$; air:$\rho_f=1.1614$ kg/m^3, $c_f=1007$ J/kg K, $k_f=0.0263$ W/m K, and $\mu=1.846\times10^{-5}$ kg/m s; sandstone [13]:$\rho_s=2200$ kg/m^3, $c_s=710$ J/kg K, $k_s=1.83$ W/m K.

The particle Reynolds number is defined as

$$\text{Re}_p = \frac{\rho_f u d_p}{\mu} \tag{51}$$

The interstitial heat transfer coefficient is expressed as [2]

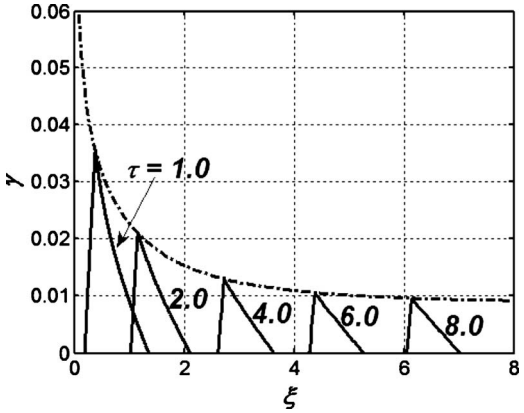

Fig. 12 Heat exchange ratio for $k=0.1$, $\beta=0.02$, $\eta_1=5$, $\theta_{in}=-0.4$, and $q_w\neq0$

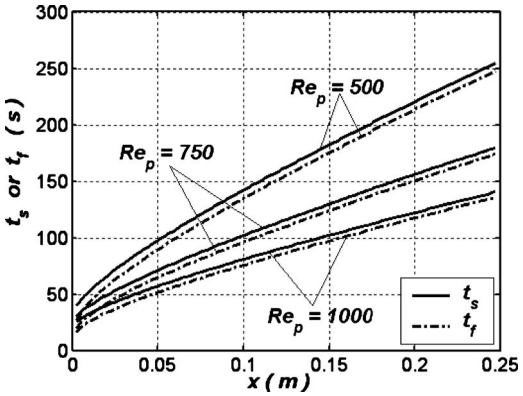

Fig. 13 Dimensional characteristic time variations of the solid and fluid phases at different Re_p for sandstone

$$h_i = \frac{k_f}{d_p}\left[2 + 1.1\ \mathrm{Pr}^{1/3}\left(\frac{\rho_f u d_p}{\mu}\right)^{0.6}\right] \tag{52}$$

The interfacial area per unit volume of the porous medium is calculated as

$$\alpha = \frac{6(1-\varepsilon)}{d_p} \tag{53}$$

The effective thermal conductivity of the fluid and solid phases of porous media are represented by

$$k_{f,\mathrm{eff}} = \varepsilon k_f \tag{54}$$

$$k_{s,\mathrm{eff}} = (1-\varepsilon)k_s \tag{55}$$

It can be seen from Fig. 13 that increasing Re_p can reduce the dimensional characteristic time for both the fluid and solid phases. However, the correlation between the dimensional characteristic time and Re_p is nonlinear.

6 Conclusions

Transient heat transfer in a packed bed subject to a constant temperature boundary condition is investigated analytically. A transient LTNE model, which incorporates diffusion in both the solid and fluid phases, is employed to represent heat transport. Exact solutions for transient solid and fluid temperature distributions, as well as steady solid and fluid temperature distributions, are derived. Exact solutions of fluid, solid, and total Nusselt number for fully developed region under steady state condition are also obtained. The results show a substantial two-dimensional thermal behavior for the solid and fluid phases, and the LTE model is found to be unsuitable to describe the transient heat transfer process in porous media. The phenomenon of heat flux bifurcation for the solid and fluid phases at the wall is found to occur over a given axial region at a given time frame. Heat flux bifurcation is also found to occur along the channel. The bifurcation region moves downstream with time and is dependent on the pertinent parameters k, β, and θ_{in}. The nondimensional axial length scale, ξ, introduced earlier can be used to represent the indirect integrated influences of Darcy and particle Reynolds numbers on the temperature difference between the solid and fluid phases. Thermal conduction at the wall is found to play an important role on the total exchange between the solid and fluid phases within heat flux bifurcation region, especially for small η_1 and large k. When $\xi > \tau/\beta$, it is found that the heat transfer can be described using the LTNE model with no convection in the fluid phase energy equation. A characteristic time is introduced to evaluate the time that it takes for either the solid or fluid to reach steady state. This characteristic time is found to increase with an increase in k, β, η_1, or θ_{in}.

Nomenclature

- Bi = $\mathrm{Bi}=h_i\alpha H^2/k_{s,\mathrm{eff}}$, Biot number
- c = specific heat (J kg^{-1} K^{-1})
- d_p = particle diameter (m)
- h_i = interstitial heat transfer coefficient (W m^{-2} K^{-1})
- H = half height of the channel (m)
- I_0 = modified Bessel functions of the first kind of zero order
- I_1 = modified Bessel functions of the first kind of order 1
- k = $k=k_{f,\mathrm{eff}}/k_{s,\mathrm{eff}}$, ratio of the fluid effective thermal conductivity to that of the solid, defined by Eq. (5)
- k_f = thermal conductivity of the fluid (W m^{-1} K^{-1})
- $k_{f,eff}$ = effective thermal conductivity of the fluid (W m^{-1} K^{-1})
- k_s = thermal conductivity of the solid (W m^{-1} K^{-1})
- $k_{s,eff}$ = effective thermal conductivity of the solid (W m^{-1} K^{-1})
- m = Laplace transform parameter
- Nu = Nusselt number
- q_w = Total heat flux at the wall (W m^{-2})
- $Q(\tau)$ = unit step function defined by Eq. (18)
- Q_i = integrated internal heat exchange between the solid and fluid phases (W m^{-2})
- Q_o = heat exchange between the solid and fluid phases through thermal conduction at the wall (W m^{-2})
- Pr = Prandtl number
- Re_p = particle Reynolds number
- s_n = $s_n=(n+0.5)\pi/\eta_1$
- t = time (s)
- T = temperature (K)
- T_0 = initial temperature (K)
- u = fluid velocity (m s^{-1})
- U = function of ξ and τ, defined by Eqs. (6) and (7)
- V = function of η, defined by Eqs. (6) and (7)
- W = Laplace transformation of U
- x = longitudinal coordinate (m)
- y = transverse coordinate (m)

Greek Symbols

- α = interfacial area per unit volume of the porous medium (m^{-1})
- ε = porosity
- β = $\beta=\varepsilon\rho_f c_f/(1-\varepsilon)\rho_s c_s$, parameter defined by Eq. (5)
- η = nondimensional transverse coordinate, defined by Eq. (5)
- η_1 = $\eta_1=H/\sqrt{k_{s,\mathrm{eff}}/(h_i\alpha)}$, nondimensional half height of the channel, defined by Eq. (5)
- ξ = $\xi=xh_i\alpha/\rho_f c_f u$, nondimensional axial length scale, defined by Eq. (5)
- θ = $\theta=(T-T_w)/(T_0-T_w)$, nondimensional temperature, defined by Eq. (5)
- μ = dynamic viscosity (kg m^{-1} s^{-1})
- ρ = density (kg m^{-3})
- γ = heat exchange ratio, defined by Eq. (49)
- Ω_w = dimensionless total heat flux at the wall, defined by Eq. (46)
- τ = $\tau=h_i\alpha t/(1-\varepsilon)\rho_s c_s$, nondimensional time, defined by Eq. (5)
- τ_f = nondimensional characteristic time for fluid phase

τ_s = nondimensional characteristic time for solid phase

Subscripts

d = fully developed
f = fluid phase
in = inlet
NC = without convection term in the fluid phase
s = solid phase, steady state
t = total
w = wall
o = initial

Superscripts

a = transverse average

References

[1] Lee, D. Y., and Vafai, K., 1999, "Analytical Characterization and Conceptual Assessment of Solid and Fluid Temperature Differentials in Porous Media," Int. J. Heat Mass Transfer, **42**, pp. 423–435.

[2] Alazmi, B., and Vafai, K., 2002, "Constant Wall Heat Flux Boundary Conditions in Porous Media under Local Thermal Non-Equilibrium Conditions," Int. J. Heat Mass Transfer, **45**, pp. 3071–3087.

[3] Amiri, A., and Vafai, K., 1998, "Transient Analysis of Incompressible Flow Through a Packed Bed," Int. J. Heat Mass Transfer, **41**, pp. 4259–4279.

[4] Schumann, T. E. W., 1929, "Heat Transfer: Liquid Flowing Through a Porous Prism," J. Franklin Inst., **208**, pp. 405–416.

[5] Riaz, M., 1977, "Analytical Solution for Single- and Two-Phase Models of Packed-Bed Thermal Storage Systems," ASME J. Heat Transfer, **99**, pp. 489–492.

[6] Spiga, G., and Spiga, M., 1981, "A Rigorous Solution to A Heat Transfer Two Phase Model in Porous Media and Packed Beds," Int. J. Heat Mass Transfer, **24**, pp. 355–364.

[7] Kuznetsov, A. V., 1994, "An Investigation of a Wave of Temperature Difference Between Solid and Fluid Phases in a Porous Packed Bed," Int. J. Heat Mass Transfer, **37**, pp. 3030–3033.

[8] Kuznetsov, A. V., 1997, "A Perturbation Solution for Heating a Rectangular Sensible Heat Storage Packed Bed With a Constant Temperature at the Walls," Int. J. Heat Mass Transfer, **40**, pp. 1001–1006.

[9] Hendal, R., Quesnel, W., and Saghir, Z., 2008, "Analytical Solution of the Thermal Behavior of a Circulating Porous Beat Exchanger," Fluid Dyn. Mater. Process., **4**, pp. 237–243.

[10] Beasley, D. E., and Clark, J. A., 1984, "Transient Response of a Packed Bed for Thermal Energy Storage," Int. J. Heat Mass Transfer, **27**, pp. 1659–1669.

[11] Yang, K., and Vafai, K., 2010, "Analysis of Temperature Gradient Bifurcation in Porous Media—An Exact Solution," Int. J. Heat Mass Transfer, **53**, pp. 4316–4325.

[12] Vafai, K., and Tien, H. C., 1989, "A Numerical Investigation of Phase Change Effects in Porous Materials," Int. J. Heat Mass Transfer, **32**, pp. 1261–1277.

[13] Vafai, K., and Sozen, M., 1990, "Analysis of Energy and Momentum Transport for Fluid Flow Through a Porous Bed," ASME J. Heat Transfer, **112**, pp. 690–699.